New family of graphene-based organic semiconductors: An investigation of photon-induced electronic structure manipulation in half-fluorinated graphene

Andrew L. Walter,[1,2,3,*] Hasan Sahin,[4] Jun Kang,[4] Ki-Joon Jeon,[5] Aaron Bostwick,[1] Seyda Horzum,[4] Luca Moreschini,[1] Young Jun Chang,[6] Francois M. Peeters,[4] Karsten Horn,[2] and Eli Rotenberg[1]

[1]*Advanced Light Source (ALS), E. O. Lawrence Berkeley National Laboratory, Berkeley, California 94720, USA*

[2]*Department of Chemical Physics, Fritz-Haber-Institut der Max-Planck-Gesellschaft, Faradayweg 4–6, 14195 Berlin, Germany*

[3]*Donostia International Physics Centre, Paseo Manuel de Lardizabal, 4. 20018 Donostia-San Sebastian, Spain*

[4]*Department of Physics, University of Antwerp, Groenenborgerlaan 171, B-2020 Antwerpen, Belgium*

[5]*School of Electrical Engineering, University of Ulsan, Namgu, Ulsan, 680-749, South Korea*

[6]*Department of Physics, University of Seoul, Seoul, 130-743, Korea*

(Received 24 October 2015; revised manuscript received 27 January 2016; published 29 February 2016)

The application of graphene to electronic and optoelectronic devices is limited by the absence of reliable semiconducting variants of this material. A promising candidate in this respect is graphene oxide, with a band gap on the order of ∼5 eV, however, this has a finite density of states at the Fermi level. Here, we examine the electronic structure of three variants of half -fluorinated carbon on Sic(0001), i.e., the $(6\sqrt{3} \times 6\sqrt{3})$ $R30^\circ$ C/SiC "buffer layer," graphene on this $(6\sqrt{3} \times 6\sqrt{3})$ $R30^\circ$ C/SiC buffer layer, and graphene decoupled from the SiC substrate by hydrogen intercalation. Using angle-resolved photoemission, core level photoemission, and x-ray absorption, we show that the electronic, chemical, and physical structure of all three variants is remarkably similar, exhibiting a large band gap and a vanishing density of states at the Fermi level. These results are explained in terms of first-principles calculations. This material thus appears very suitable for applications, even more so since it is prepared on a processing-friendly substrate. We also investigate two separate UV photon-induced modifications of the electronic structure that transform the insulating samples (6.2-eV band gap) into semiconducting (∼2.5-eV band gap) and metallic regions, respectively.

DOI: 10.1103/PhysRevB.93.075439

I. INTRODUCTION

The unusual electronic properties of graphene have attracted an enormous interest within the last few years [1–6]. Faraday rotation in graphene [7], graphene-based electronics [1,8,9], and graphene terahertz plasmon oscillator [10] research has provided a basis for the application of graphene, but despite all this research organic molecular films still provide the best candidates for carbon-based electronics [11–13].

Many efforts have been directed at introducing a band gap in graphene, to render it semiconducting, for example, by varying the amount of oxidation [14] in a graphene sheet which has led to a system with a ∼5-eV band gap, but this material has a finite density of states at the Fermi level, making it less desirable for electronic applications.

Recently, we showed that the combination of electronic structure exhibited in organic films [11–13], including a vanishing density of states at the Fermi level, the benefits of large defect-free films, as observed for graphene on SiC, the ability to pattern using UV/x-ray photons and the ability to produce samples in an industrially friendly manner was observed in half-fluorinated graphene on hydrogen-terminated SiC [15]. In this paper, we extend this research, showing that the choice of substrate-film interface has little effect on the electronic structure of such films. We take a closer look at the UV photon-induced modification process, an essential property allowing for patterning of the π bands (∼2.5-eV band gap) on a semi-insulating (∼6.3-eV band gap) substrate. In addition, we investigate the second, independent, UV photon-induced variation which allows for patterning of metallic regions on the same sample. As common lithographic processes can pattern at the nanometer scale using UV photons, devices consisting of nanometer-size semi-insulating (∼6.2 eV), semiconducting (∼2.5 eV), and metallic regions are thus possible.

Our earlier study of half-fluorinated graphene sheets presented in the previous work [15] demonstrated that all desirable properties are realized in this new material: (i) the films have a 2.5-eV band gap and readily emit visible light in the blue region on mild heating; (ii) photon-induced sample charging is observed, indicating a vanishing density of states at the Fermi level; (iii) graphene produced on the SiC(0001) face has a demonstrated high quality and is ideally suited to industrial production [16–18], while the fluorination process is also easily transferred to industrial scale; (iv) the conduction and valence bands are susceptible to UV light, making standard lithography patterning techniques possible. All of these properties indicate the potential of this new functionalization of graphene and all three of the substrate-film interfaces investigated in this work share these properties. In addition, the marked similarity of other functionalized graphene samples (notable G-O [14] and G-H [19,20]) provides strong evidence that future G_2-X, X being any attached atomic species, systems will help to strongly vary the band gap in the semi-insulating and semiconducting regions, providing a strong candidate for the realization of graphene-based electronics. In fact, theoretical studies have concluded that half-hydrogenation of graphene should allow for the conduction and valence bands, similar to those observed in the current samples, to be spin polarized [19,20], opening the door to integrated spintronic devices.

*Corresponding author: awalter@bnl.gov; Present address: Brookhaven National Laboratory, National Synchrotron Light Source II, Upton, New York, 11973.

We present core level x-ray photoemission spectra (XPS), angle-resolved photoemmission spectra (ARPES), near-edge x-ray absorption fine structure spectra (NEXAFS), and photon irradiation dependent photo-emission (pidPES) on half-fluorinated quasifreestanding graphene, graphene on $(6\sqrt{3} \times 6\sqrt{3})$ $R30^\circ$ C and $(6\sqrt{3} \times 6\sqrt{3})$ $R30^\circ$ C samples on silicon-terminated SiC(0001) substrates. The carbon atoms in graphene are sp^2 bonded in a two-dimensional (2D) hexagonal lattice, so-called σ bonds. The p orbitals perpendicular to the plane form a delocalized π bonding network, known as π bonds. In fully functionalized graphene, each alternating carbon atom has the, formerly, π bonds above (below) the plane, respectively, attaching hydrogen [21,22] or fluorine [19,20,23] to each of these bonds results in a semiconducting material with a band gap of $\geqslant 3$ eV. However, attaching fluorine to one side only results in the formation of two flat, localized, bonding/antibonding states above and below the Fermi level, respectively, after extreme ultraviolet (EUV) photon irradiation. Although this results in both the σ and π bands obtaining a strong sp^3 character, for ease of description we will continue to call the electronic bands resulting from these bonding atoms as σ and π "states," this is done mainly because the formerly σ bands in the graphene structure are relatively unchanged on half-functionalization, while the formerly π bands are strongly influenced. The two flat, localized, states are similar to the HOMO and LUMO levels in organic electronic materials [11–13]. This was attributed to transitions between a ground-state configuration and a metastable configuration resulting in defect states. We show that the film-substrate interface has little effect on the electronic structure and investigate two separate EUV photon-induced modifications that transform the semi-insulating samples(∼6.3-eV band gap) into semiconducting (∼2.5-eV band gap) and metallic regions, respectively. These new samples are therefore perfectly suited for implementation in graphene-based electronic devices.

II. METHODS

Experiments were performed on quasifreestanding graphene, graphene on $(6\sqrt{3} \times 6\sqrt{3})$ $R30^\circ$ C and $(6\sqrt{3} \times 6\sqrt{3})$ $R30^\circ$ C samples on silicon-terminated SiC(0001) substrates. The $(6\sqrt{3} \times 6\sqrt{3})$ $R30^\circ$ C layer (henceforth $6\sqrt{3}$ C) layer is a covalently bound, electrically inactive graphene layer [24] in which about one third of the C atoms bind to the Si atoms on the SiC(0001) substrate. This bonding breaks up the π band network so that the $6\sqrt{3}$ C layer has no Dirac cone. The $6\sqrt{3}$ C/SiC samples were prepared with the method of Emtsev *et al.* [24] which involves annealing of SiC in an Ar atmosphere. The graphene on $6\sqrt{3}$ C/SiC (henceforth G/$6\sqrt{3}$ C-SiC) was prepared in the same method, with a higher annealing temperature [24]. Quasifreestanding graphene (henceforth G/H-SiC) was prepared from a $6\sqrt{3}$ C/SiC sample by the method of Riedl *et al.* [25] where annealing in a hydrogen atmosphere intercalates hydrogen between the $6\sqrt{3}$ C layer and the substrate, decoupling the carbon layer producing quasifreestanding graphene films.

Samples were fluorinated following a method similar to that of McFeely *et al.* [26] whereby samples are placed in a reaction chamber with a XeF_2 crystal and heated to 200° C for 2 h, leading to the dissociation of the XeF_2 and the liberation of reactive fluorine atoms. This method has previously been used to study the interaction between fluorine and silicon surfaces [26] as well as fluorine and graphene [23,27–29] and leads to the formation of C-F bonds with the graphene layer. After annealing, the $6\sqrt{3}$ C-SiC, G/$6\sqrt{3}$ C-SiC, and G/H-SiC samples will be labeled as F-$6\sqrt{3}$ C/SiC, F-G-$6\sqrt{3}$ C/SiC, and F-G/H-SiC, respectively.

ARPES, NEXAFS, XPS, and pidPES spectra were obtained at the Electronic Structure Factory end station (SES-R4000 analyzer) at beamline 7 of the Advanced Light Source, Lawrence Berkeley National Laboratory. The spatial area sampled in these measurements was typically 50 to 100 μm. During the measurements, the samples were cooled to ∼100 K using a liquid-He-cooled cryostat and the pressure was $<2 \times 10^{-10}$ Torr. A photon energy of 95 eV was used in the ARPES measurements giving overall resolutions of ∼25 meV and ∼0.01 Å^{-1}.

First-principles calculations were performed using the VASPcode [30,31]. The projector augmented wave (PAW) method [32,33] and the generalized gradient approximation of Perdew-Burke-Ernzerhof [34] (GGA-PBE) are adopted. The energy cutoff is set to 400 eV and the k-grid mesh is $9 \times 9 \times 1$. Structural relaxation was stopped when the force acting on each atom was less than 0.01 eV/Å. Van der Waals interaction were included by using the DFT-D2 approach [35]. The vacuum layer was larger than 10 Å to avoid interaction between periodic images. Dipole correction is applied to eliminate the effect of artificial electronic field imposed by the periodic boundary condition. In the calculations, the SiC substrate contains four SiC layers, and the two bottom layers were kept fixed. The dangling bonds at the bottom surface are passivated by H atoms. The work function is determined as the energy difference between the Fermi level and the vacuum level at the half-fluorinated graphene side. Charge transfer is calculated based on the Bader charge analysis [36].

III. RESULTS

A. Physical and chemical structure

The structure of the F-G/H-SiC sample has been shown to consist of fluorine attached to one side of the graphene layer [15]; a schematic is shown in Fig. 1(a). The existence of similar dangling bond states, as revealed in ARPES data (below), in the F-$6\sqrt{3}$ C/SiC and F-G-$6\sqrt{3}$ C/SiC samples suggests a similar fluorinated structure. The side view of the F-G/H-SiC sample is presented in Fig. 1(c), where the H terminates the SiC dangling bonds and the resulting C_2F film is decoupled from the substrate. A similar structure is proposed for the F-$6\sqrt{3}$ C/SiC structure [Fig. 1(b)], although the Si dangling bonds remain. Complete fluorination of bilayer graphene has been theoretically shown to result in sp^3 bonding between the two graphene layers [38] forming a C_4F film; we therefore propose a similar structure for the F-G-$6\sqrt{3}$ C/SiC sample, shown in Fig. 1(d).

The extent of bonding between the two types of films in Figs. 1(b) and 1(d) and the substrate is investigated using XPS. All three samples are observed to emit blue light, after exposure to UV photons and subsequent light annealing, as a result we conclude that the ground-state configuration and metastable configuration observed previously [15] are

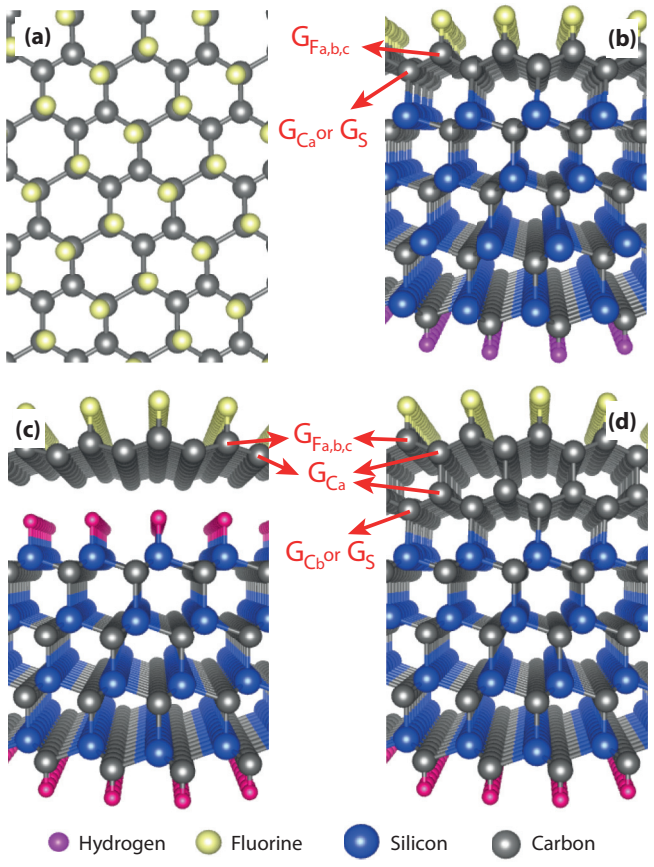

FIG. 1. A perspective view of the structure of the top layer of all three samples (a) and a side view of the half-fluorinated $6\sqrt{3}$C-SiC (b), half-fluorinated G/H-SiC (c), and the half-fluorinated G/$6\sqrt{3}$C-SiC (d). Fluorine atoms are shown in yellow, hydrogen in pink, carbon in gray, and silicon in blue.

attributed to all three. In addition, all three have a photon-induced C 1s component ($G_{F(c)}$ in Fig. 2) which is observed after exposure to UV photons. This was previously shown [15] to be related to the metastable state, and provides further evidence of a similar ground and metastable state in all three samples.

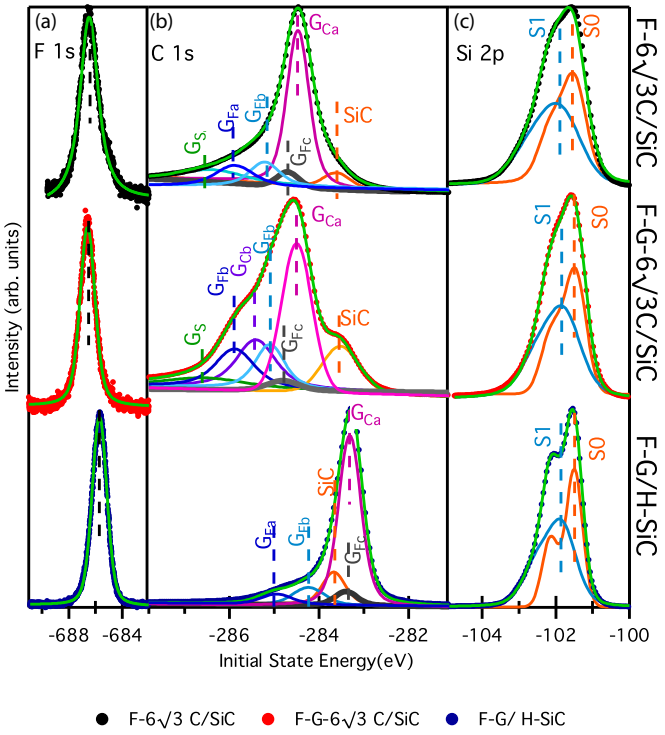

FIG. 2. XPS spectra obtained from the three samples: F-$6\sqrt{3}$ C/SiC (black circles), F-G-$6\sqrt{3}$ C/SiC (red circles), and F-G/H-SiC (blue circles). Overview scans (not shown) indicate only C, F, and Si present in the samples except for a small (<2%) O contamination. Detailed F 1s (a), C 1s (b), and Si 2p (c) are also shown, with fitted peaks (solid colored lines) and fitted spectra (solid green lines).

An overview XPS spectra was obtained from each of the three samples (not shown) which indicates only that F, C, and Si are present, except for a small (<2%) oxygen contamination. Detailed XPS spectra from the three samples are presented in Fig. 2 with least-squares-fitted components also included. In addition, the fitted component peak positions are listed in Table I along with the positions of the peaks prior to fluorination. To provide a greater insight, we include in Table II the calculated work function (WF) and the calculated charge

TABLE I. XPS fitted peak positions (eV) for the three samples investigated before and after fluorination. The C 1s peaks in the fluorinated samples are assigned, in agreement with the structures in Fig. 1, as G_{Ca}-C bonded to C,G_{Ca}-C bonded to C close to the substrate (F-G-$6\sqrt{3}$ C/SiC only), $G_{F(a/b)}$-C bonded to F in the ground configuration, $G_{F(c)}$-C bonded to F in the metastable configuration, G_S-C bonded to the substrate. *Note: For the unfluorinated samples G_{Cb} is the buffer layer C-C bonded component, G_{Fa} is the graphene component, and G_S is the C bonded to the substrate component.

Energy (eV)	F 1s	C 1s						Si 2s	Si 2p	
Sample		G^*_S	G^*_{Cb}	$G^*_{F(a/b)}$	G_{Ca}	SiC	G_{Fc}		S1	S0
$6\sqrt{3}$ C-SiC		−284.75 [24]	−285.55 [24]			−283.7 [24]		−152.5 [25]	101.7 [37]	−101.4 [37]
F-$6\sqrt{3}$ C/SiC	−686.5	−286.34		−285.70/ 284.98	−284.49	−283.7	−284.71	−152.5	−101.6	−101.3
G/$6\sqrt{3}$ C-SiC		−284.75 [24]	−285.55 [24]	−284.75 [18]		−283.7 [24]		−152.5 [25]	−101.7 [37]	−101.4 [37]
F-G-$6\sqrt{3}$ C/SiC	−686.5	−286.40	−285.13	−285.72/ 284.96	−284.51	−283.7	−284.72	−152.5	−101.6	−101.3
G/H-SiC				−284.6 [25]		−283.0 [25]		−151.8 [25]	−100.9 [25]	− 100.6 [25]
F-G/H-SiC	−685.5			−284.99/ 284.23	−283.27	−283.7	−283.40	−152.5	−101.6	−101.3

TABLE II. Table showing the work function and charge transfer between the substrate and the F-G layers for each of the substrates calculated by DFT as explained in the Methods section. The amount of the additional (donated) electron is shown by minus (plus) sign.

Energy (eV) Sample	WF	Charge transfer F layer	1st C layer	2nd C layer	C substrate
F-6$\sqrt{3}$ C/SiC	7.21	+0.1	+1.7		−1.8
F-G-6$\sqrt{3}$ C/SiC	7.27	+0.2	−0.1	+1.5	−1.6
F-G/H-SiC	8.36	0	0		0

transfer between the various layers for comparison to the XPS spectra. The F 1*s* peaks consist of only one component in all three cases, indicating that a single chemical species is present, consistent with the structures proposed in Fig. 1. The only difference in the F peak is a shift of ∼1 eV to lower binding energy for the F-G/H-SiC sample. This is consistent with an increase in the calculated work function of this sample by ∼1 eV compared to the two others. The Si 2*p* peak has two doublet peaks (labeled S0, bulk component, and S1, surface component) as described by Carlisle *et al.* [39], the adatom component (S2) is not present due to the lack of adatoms on the surface after graphene growth. The Si 2*p* peaks are similar for all three samples, and similar to the unfluorinated 6$\sqrt{3}$ C-SiC and G/6$\sqrt{3}$ C-SiC. The relative shift of the unfluorinated G/H-SiC (of ∼0.7 eV) may indicate that the H layer is removed during the fluorination process. However, this would lead to a sample indistinguishable from the F-6$\sqrt{3}$ C/SiC, which does not agree with the F 1*s* and the C 1*s* peaks (discussed in the following). Our calculations indicate that, similar to the G/H-SiC case, no charge transfer is likely to occur between the H-SiC substrate and the F-G layer. We propose, however, that the Si 2*p* XPS data indicate that for F-G/H-SiC charge transfer between the substrate and the F-G film does occur.

Let us now turn to a detailed analysis of the C 1*s* peak shape. The C 1*s* peak has the following components: from the substrate (SiC), for C-C bonded species (G_{Ca}), C-C bonded species close to the SiC substrate (G_{Cb}), C bonded to F in the ground configuration (G_{Fa} and G_{Fb}), C bonded to the SiC substrate (G_S), and a photon-derived C species (G_{Fc}) which is attributed to the C bonded to F in the metastable configuration. The location of each of the atomic species is indicated in Fig. 1 while the atomic ratios of each component are presented in Table III. Interestingly, it appears that the fluorination process reduces the number of graphene-substrate bonds for the F-6$\sqrt{3}$ C/SiC and the F-G-6$\sqrt{3}$ C/SiC samples, as only 4% of the C atoms (Table III, G_S peak) are now bonded to the substrate (∼33% and ∼16% originally). This indicates a reduction in the substrate-film interaction upon fluorination.

It is perhaps important to note here that the XPS fitting was performed without considering the number of "expected" components and the number of peaks is the minimum number that provided a good description of the measured data. During the fitting all parameters of all peaks (energy, amplitude, Lorentzian width, Gaussian width, asymmetry) where "free." The results of the fitting therefore indicate that the calculated structures shown in Fig. 1 are not entirely accurate, in fact,

TABLE III. Atomic ratios for the different species, scaled from XPS fitted peak areas using the calculated photoemission cross sections [43], for the three samples after fluorination. The expected values (in parentheses and italics) are determined based on the observed $G_{Fa,b,c}/(G_{Ca,b}+G_S)$ ratio, the observed substrate bonding ratio (G_S) and the structures presented in Fig. 1.

Atomic conc. (ratios)	F-G/H-SiC Obs. (Exp.)	F-6$\sqrt{3}$ C/SiC Obs. (Exp.)	F-G-6$\sqrt{3}$ C/SiC Obs. (Exp.)
F/G peaks	0.28 *(0.33)*	0.39 *(0.37)*	0.16 *(0.17)*
G_{Fa}	0.12 *(0.13)*	0.09 *(0.10)*	0.09 *(0.07)*
G_{Fb}	0.12 *(0.13)*	0.08 *(0.10)*	0.08 *(0.07)*
G_{Fc}	0.11 *(0.13)*	0.07 *(0.09)*	0.08 *(0.06)*
G_{Ca}	0.65 *(0.61)*	0.72 *(0.67)*	0.46 *(0.49)*
G_{Cb}	n/a	n/a	0.26 *(0.29)*
G_S	n/a	0.04 *(0.04)*	0.02 *(0.02)*

the F atoms not being centered directly over the C atoms below (see Fig. 1) perhaps leads to a slight buckling, or a slight increase/decrease, of each alternating F bonded C atom resulting in two independent C-F bonded components in the ground state. As only one F component is observed, this suggests that the high charge associated with the F atom results in a much smaller (and unobservable in the current data) shift in the F atoms.

In the F-G-6$\sqrt{3}$ C/SiC there are two Gfb components instead of one in the F-6$\sqrt{3}$ C/SiC. This is due to the presence of the extra graphenelike layer underneath (buffer layer). This component is at the same binding energy (Table I) as before fluorination, while the other C 1*s* components are the same as those observed in the F-6$\sqrt{3}$ C/SiC sample. This is in direct contrast to the calculated chemical shifts, which give a shift of ∼1.8 eV between the locations of the C peaks in the topmost layer in these two samples. The similarity of these top layer carbon line-shape components in the two samples indicates that the F atoms play the major role in these chemical shifts and not the substrate as indicated by the calculated charge transfers. A further indication of the role of the F atoms is found by considering the experimental atomic ratio, 2% of the graphene atoms (4% of the bottom layer) are now bonded to the substrate, similar to the case of F-6$\sqrt{3}$ C/SiC. An important result here is that this mechanism of charge transfer to the substrate acts to maintain the chemical state of the substrate, thereby maintaining the location of the Fermi level in the gap. While such a complicated charge transfer mechanism is not common in normal-metal semiconductor interfaces, equally complex mechanisms have been observed in organic electronic materials [11,13,40] which are closely related to graphene films.

This same mechanism is derived from the results of the F-G/H-SiC sample, where the substrate related peaks shift (−0.7 eV) from the clean SiC values[1] by a similar amount to those seen in the previous samples (Table I and Fig. 2). As described above, we rule out the removal of the H interface layer and a subsequent resumption of the graphene-substrate bonding due to the complete lack of a substrate bonding

[1]Clean SiC values are −100.8, −101.1, −151.5, and −282.7 eV [41].

component in the C 1*s* (G3) and the significant differences between the C 1*s* spectra for the F-G/H-SiC and the F-6$\sqrt{3}$ C/SiC samples. Instead, we observe a large, 1.4 eV, chemical shift of the G_{Ca} component (closest to the substrate) which we attribute to a charge transfer from the substrate to the F-G film, which is contrary to the results from the calculations. This pronounced shift results in the same chemical state (peak locations) for the SiC substrate as in the previous two samples and therefore is attributed to a Fermi level pinning commonly observed in semiconductor heterojunctions [42]. This will be discussed in more detail in the following section regarding the electronic structure.

The fluorination of the topmost graphene layer is found to be 33%, 38%, and 39% for the F-6$\sqrt{3}$ C/SiC, F-G-6$\sqrt{3}$ C/SiC, and F-G/H-SiC samples, respectively (Table III). This indicates slightly less than half-fluorinated samples, however, the use of calculated photoemission cross sections [43] is known to introduce large errors. A better approach is to compare the ratio of the C 1*s* component related to graphene bonded to F ($G_{Fa,b,c}$) to all other graphene C 1*s* components as the cross section in this case is not relevant. Expected atomic ratios based on the area of the fitted peaks and the structures presented in Fig. 1 are compared to experimental values in Table III. Good agreement is seen between the experimental and expected values in all three samples, providing strong support for the proposed structures presented in Fig. 1. Further support is given by comparing this to our previous measurements [15], where good agreement to these new samples is found. Structure assignment is strengthened in the previous paper by including photoelectron diffraction data.

The XPS analysis therefore indicates a number of important features of these samples: The fluorination of samples with film-substrate bonding acts to reduce the number of atoms bonding with the substrate, thereby reducing the film-substrate interactions. A complex charge transfer mechanism, similar to that observed in organic films [11,13,40], acts to keep the substrate peaks at the same position in all samples, despite the change in work function between the F-G/H-SiC sample and the others. Finally, the fluorination of G/6$\sqrt{3}$ C-SiC results in the formation of bonds between the fluorinated graphene layer and the 6$\sqrt{3}$ C producing a chemical structure very similar to that of F-6$\sqrt{3}$ C/SiC. As all three samples appear to have similar physical and chemical structures, it becomes relevant to ask whether they also have similar electronic structures.

B. Valence electronic structure

The similarity of the physical and chemical structure of the three samples is also apparent in the electronic structure [Figs. 3(b)–3(d)] as revealed in angle-resolved photoemission of the valence bands. The ARPES data are presented as binding energy versus wave-vector images, with the photoemission intensity indicated by a color scale; the present maps show the photoemission along the major axes in the 2D Brillouin zone of graphene. For comparison, the band structure of the 6$\sqrt{3}$ C-SiC structure prior to fluorination is also included [Fig. 3(a)], which has some differences and some similarities. As discussed in the Introduction, the hexagonal carbon structure has σ bonds and π bonds, the latter projecting out of the film plane. These form two types of valence

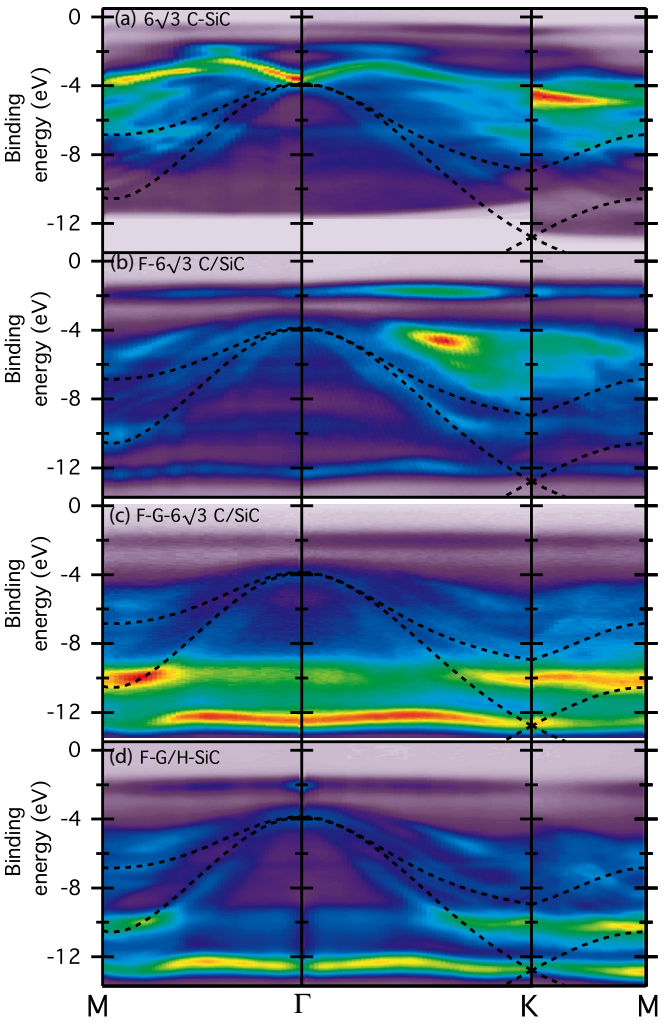

FIG. 3. ARPES spectra obtained along the three principal directions for unfluorinated 6$\sqrt{3}$ C-SiC (a), F-6$\sqrt{3}$ C/SiC (b), F-G-6$\sqrt{3}$ C/SiC (c), and F-G/H-SiC (d). As a guide to the eye, first-nearest-neighbor tight-binding calculations of graphene σ bands, performed using the parameters given by Saito *et al.* [48], are overlaid in (a)–(d) with a scaling of 0.8 and an ϵ_{2p} value of −2.4 eV.

bands, σ bands and π bands, respectively, with the π bands forming the delocalized, linear Dirac-type, bands which are commonly associated with graphene. Bonding between the graphene and a substrate or functional group (H [19,20], F [38,44,45], O [46], Si [24]) acts to destroy the delocalized π bonds, with the remaining nonbonding graphene π electrons forming localized nondispersing energy bands. For the case of 6$\sqrt{3}$ C-SiC, one third of the graphene C atoms bond to the substrate, quenching the substrate dangling bonds, with the remaining atoms forming the nondispersing localized bands observed at ∼−1.6 and ∼−0.6 eV in Fig. 3(a). Buckling of the graphene lattice results in the sp^2 bonding becoming more sp^3 like and this alters the sp and p_z character of the π and σ bands significantly. The band structure calculations, and measurements, indicate that the effect on the σ bands is small with little change to these states observed. In contrast, the π bands are strongly affected, therefore, in order to make the discussion easier to follow we will continue to use the π

and σ nomenclature despite this being not strictly true. While some of the non-π bands [those in the range -3 eV <-10 eV in Fig. 3(a)] are due to the SiC substrate or are due to the semibonding π bands in the ground configuration, for ease of discussion unless otherwise stated they will be labeled as σ bands in the following.

The most intense band in the fluorinated graphene samples is the weakly dispersing one observed to cross the Γ, K, and M points at about ~-12 and ~-10 eV [Figs. 3(b)–3(d)]. These two bands are attributed to predominantly F atom states, based on the calculations by Junkermeier *et al.* [47]. A nondispersing π band is observed in the fluorinated samples at ~-1.9 eV, however, this band only appears after photon irradiation and its intensity is related to that of the peak labeled G_{Fc} in Fig. 2(b). The origin of this band will be discussed in detail in the next section, but for now it is important to note that a second nondispersing band is observed at $\sim$0.6 eV in the $6\sqrt{3}$ C-SiC sample. As no other nondispersing band is observed in the fluorinated sample, we conclude that the band corresponding to the 0.6-eV band in $6\sqrt{3}$ C-SiC band is instead shifted above the Fermi level, a fact that is confirmed by the NEXAFS data presented in the following.

The rest of the σ bands are similar in the fluorinated samples and the $6\sqrt{3}$ C-SiC sample, further confirming the similarity of the structures. To illustrate this first-nearest-neighbor tight-binding (FNN–TB) calculations of the σ bands performed using the method and parameters of Saito *et al.* [48] are overlaid (black dashed curves in Fig. 3). This shows that the graphene σ bands are not substantially altered by fluorination. The calculated π bands are not shown as the half-fluorination process changes these significantly.

We can now turn our attention to an apparent contradiction, that is, the valence bands of the fluorinated graphene structures have the same binding energy in each of the cases, while the F-G/H-SiC sample has significantly shifted ($\sim$1 eV) graphene core levels. In the simple band-bending model of charge transfer, a ridged shift of valence and core levels is expected. Differing shifts in the valence and core levels can be explained as follows. The substrate core and valence levels undergo rigid band bending which aligns the Fermi level in the gap. The valence electrons in the fluorinated graphene layer are shifted via the interactions with the substrate discussed in the previous paragraph. These mechanisms involve screening/interaction with the substrate electric field and/or valence bands. The fluorinated graphene nuclei will screen the core level electrons from these effects much more strongly than the valence electrons, therefore, we can expect relative shifts between the core levels and the valence levels. The final step involves the dipole-induced alignment of the gaps in the semiconducting heterojunctions described by Tersoff [42] which acts to align the fluorinated graphene valence bands with the SiC valence bands.

For a deeper understanding of the electronic structure of half-fluorinated graphene on three different substrates, we also calculated band dispersions, which are presented in Fig. 4. As in the previous investigation [15], the calculations have a similar shape to the observed ARPES spectra (Fig. 3), particularly if we only consider the fluorinated graphene σ bands (in red in Fig. 4). Quantitatively, however, a large "scaling factor" of $\sim$3 is required to match the calculations with the experimental bands. This scaling factor applies to the entire band structure

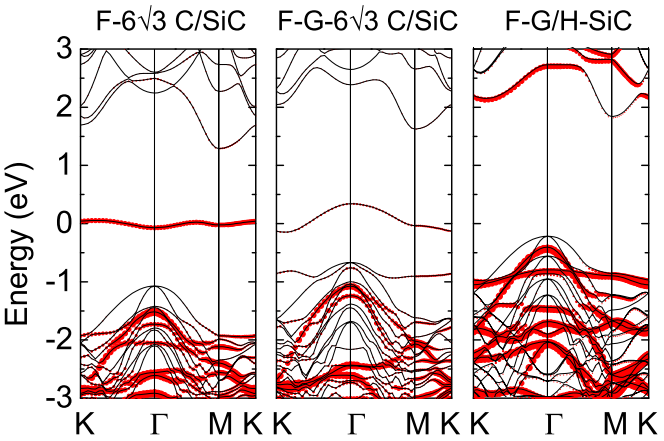

FIG. 4. The band structures of the three different structures. The red dots indicate the contribution from the half-fluorinated graphene.

and not just the band gap. In the following discussion, we will restrict ourselves to the fluorinated graphene (red) bands as these appear to be the most visible bands in the ARPES spectra. The F-$6\sqrt{3}$ C/SiC and the F-G-$6\sqrt{3}$ C/SiC calculations are particularly similar, as is observed experimentally. The main difference is a new flat band appearing at the Fermi level in the F-$6\sqrt{3}$ C/SiC case, which is not observed in the ground-state spectra experimentally, recalling that the flat band at $\sim$2 eV in Fig. 3 only appears after photon irradiation. Instead, we observe something similar for the F-G-$6\sqrt{3}$ C/SiC calculations in both cases. This we attribute to the calculations not correctly predicting the bonding between the F-$6\sqrt{3}$ C and the SiC substrate, indicated by the XPS spectra. This is most likely a result of the incomplete fluorination and the small substrate-sample bonding observed in the experimental samples that breaks up the π bonding network and is the origin of this flat band. The final structure F-G/H-SiC also has a similar calculated spectra, however, it is shifted $\sim$1.4 eV closer to the Fermi level. As described above, we believe that a core level screening process shifts the valence band relative to the core levels in this case, placing the Fermi level in the gap of the F-G. This results in a similar positioning of the bands for all three substrates investigated.

An important test of the current description of the occupied electronic structure in systems which have one graphene sublattice sp^3 bonded to a functional group is to compare the calculated σ bands of a number of these systems. These σ bands, with their energy maxima at Γ, should be very similar as we only observe major differences in the π bands between the $6\sqrt{3}$ C-SiC sample and the fluorinated samples. While published calculations of half-functionalized graphene systems have been limited to hydrogenation [20,44,49], the study of fully functionalized systems has been much wider. Fully hydrogenated [21,49], fluorinated [44,45], and half-hydrogenated–half-fluorinated graphene [44] have all been shown to have very similar electronic structures which are dominated by the σ bands and two sets of bonding π bands. This is confirmed by our own calculations in Fig. 4. All of these calculations [44,49] show that full or half-hydrogenated samples have very similar band structures, with the addition of a second set of bonding π bands expected for the fully

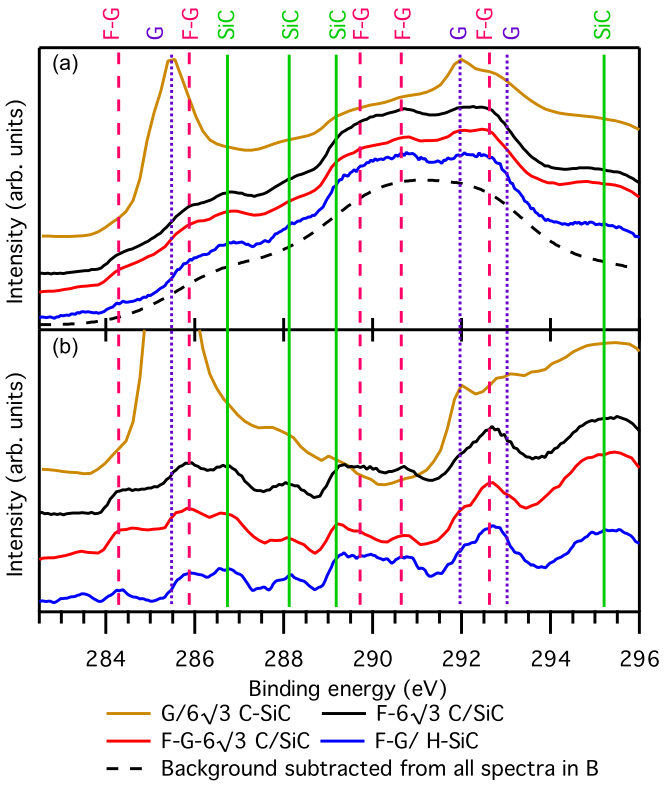

FIG. 5. NEXAFS measurements of the unoccupied states on the F-6$\sqrt{3}$ C/SiC (black), F-G-6$\sqrt{3}$ C/SiC (red), F-G/H-SiC (blue), and unfluorinated G/H-SiC. The spectra in (b) have had the polynomial background [black dashed line in (a)] subtracted from the spectra in (a) to highlight the peaks. Vertical lines highlight the peaks related to fluorinated graphene (dashed line, pink), unfluorinated graphene (dotted line, purple), and substrate (solid line, green).

hydrogenated case and a second set of σ bands and a set of nonbonding π bands in the half-hydrogenated case. The second set of σ bands in the half-hydrogenated case is due to the loss of sublattice symmetry associated with bonding to one sublattice only.

In order to investigate the unoccupied states in the fluorinated samples, NEXAFS measurements were recorded (Fig. 5) and compared to that for unfluorinated G/6$\sqrt{3}$ C-SiC. In order to enhance the discussion of the NEXAFS, we present a quick description of how ARPES and NEXAFS spectra are connected. ARPES spectra provide the unoccupied band structure, including the energy and momentum. NEXAFS, on the other hand, measures the unoccupied states providing a momentum-integrated measure of these states. So, the first requirement to compare the two is to integrate (or sum) the ARPES data along the momentum axis. We now have a series of peaks at various energies in both data sets which are related. The intensities of the two measurements, however, are not comparable.

In order to highlight the peaks in the spectra in Fig. 5(a), a polynomial background (dashed black line) has been subtracted from each spectra, with the results presented in Fig. 5(b). Each of the observed peaks is then labeled as F-G (only observed in fluorinated samples), G (only observed in the unfluorinated sample), or SiC (observed in all samples). Comparison of the F-G labeled peaks to the band crossings at Γ in Figs. 3(b)–3(d) allows the assignment of the first (lowest energy), second, fourth, and fifth NEXAFS states to similar, but not identical, ARPES states (the calculations show that the occupied states have a similar, but not symmetric, unoccupied bands). NEXAFS is an angle-integrating technique, therefore, the third NEXAFS peak can be associated with the ARPES band which curves down to cross the K and M points close to the flat band at $\sim$10 eV.

Variations in localized states have been extensively studied in organic electronic films [11,13] with a decrease in separation of the localized π states (henceforth "gap") related to an enhanced screening of the photohole via the substrate electric field. An important aspect of this process is that the center of the gap between the two localized levels remains constant with energy. A second process, which acts to shift the gap center, occurs due to the partial metallization and hybridization of localized orbitals in the organic (graphene) layer and this process can shift the usually unoccupied upper localized state below the Fermi level. In the current investigation, it is expected that, due to the 6$\sqrt{3}$ C-SiC bonding, the SiC-C film separation distance will be smaller than in the fluorinated samples and, hence, both of these processes which act on the localized states will have a greater effect. This leads to a much smaller separation of the localized states and a shift of the upper state below the Fermi level in 6$\sqrt{3}$ C-SiC. Importantly, in this case the variation of the gap size between fluorinated samples and the 6$\sqrt{3}$ C-SiC is an order of magnitude larger than observed in any organic film layer. This is most likely due to the large gap between the fluorinated localized π bands and the strong 6$\sqrt{3}$ C substrate interactions in the unfluorinated sample.

We thus arrive at a consistent picture of the chemical, physical, and electronic structure of the three fluorinated samples. Each one has fluorine bonded to one sublattice of the graphene, which results in σ bands, bonding π bands, and nonbonding localized π states. In the ground state, these dangling bonds form semibonding pairs which act to buckle the films, resulting in every second row of F bonded C atoms being pushed above the plane in the "boat" structure. This pairing also removes the localized dangling bond states. A second, photon-induced, metastable state is also observed which has the localized dangling π band states. Fermi level pinning acts to align the band gaps of the fluorinated graphene and SiC and sets the Fermi level within the gap. Relative shifts in the valence and core levels are attributed to partial core level screening, similar to what has been observed in organic electronic films. The occupied states have corresponding unoccupied levels and the proposed interpretation is supported by calculations. In addition, the same mechanisms can explain the electronic structure of the related 6$\sqrt{3}$ C-SiC, where two thirds of one graphene sublattice bond to the substrate. The one omission from the current discussion has been the nondispersing state at ~-1.9 eV and its unoccupied counterpart at $\sim$0.6 eV; as mentioned, these are photon-induced states and a discussion of the photon-induced modifications will complete the understanding of the system.

C. Photon-induced modifications

In our earlier study [15] of half-fluorinated graphene on the H-passivated SiC(001) surface, we found two separate

photon-induced modifications of the electronic band structure. The first occurs upon low-intensity irradiation (90-eV photons) with small doses, and induces a transformation from the stable conformation to a metastable structure that is characterized by the appearance of new emission lines in the valence and core level spectra. This transformation acts to reduce the band gap from ∼6 to ∼2.5 eV. This metastable phase reverts back to the ground state, under emission of blue light. The second process involves the removal of the fluorine atoms by intense UV irradiation with high doses (zero-order light consisting of a large range of photon energies). This causes exposed regions to revert back to the metallic graphene film. Both of these mechanisms are important: the first allows for regions of small band-gap semiconductor to be patterned, while the second allows for regions of unfluorinated graphene or $6\sqrt{3}$ C to be patterned. Both of these processes appear to produce regions which are limited in size by the photon spot, which means that the application of standard lithography techniques should be able to pattern the regions at the nanometer scale.

The investigation of the low-intensity photon variation using photon-based techniques required a complicated measurement procedure. Spectra were obtained over the C 1*s* edge using very low flux and very short exposure times (millisecond range), to slow the photon-induced modifications, by measuring the valence band as a function of photon energy in 0.01-eV steps between 282 and 294 eV. Several spectra were then obtained sequentially with the beam blocked from hitting the sample between measurements. In this way, we were able to obtain valence band spectra as a function of photon exposure time. Concurrently with the acquisition of the valence band photoemission spectra at each photon energy, the current to ground was recorded, which gives the NEXAFS spectra also as a function of exposure time.

In addition to the occupied bands from the ARPES spectra, and the unoccupied spectra from the NEXAFS at the same time we can obtain the second-order core level, which corresponds to XPS spectra of the C 1*s* core level taken with second-order photons (photons with twice the energy of the photon energy

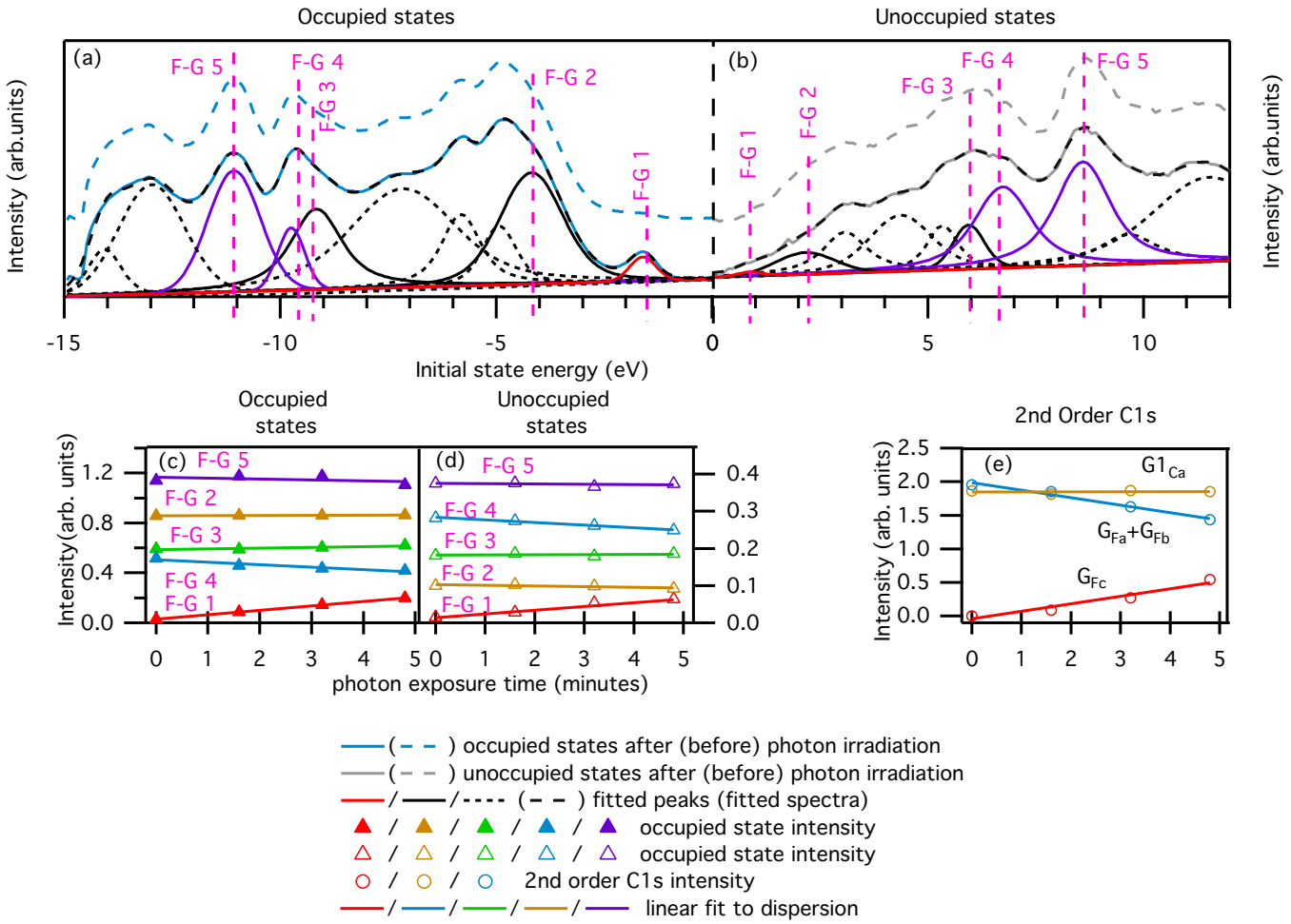

FIG. 6. The occupied (a) and unoccupied (b) states of the fluorinated G/H-SiC before, dashed blue/gray lines, and after, solid blue/gray lines, photon irradiation measured using angle-integrated photoemission and NEXAFS, respectively. A fit to the after irradiation spectra (dashed, black) and the corresponding peaks (dotted/dashed, black) are shown, with the peaks corresponding to the fluorinated graphene highlighted in solid black (C derived), purple (F derived), and red (localized dangling π bond) lines. The variation of the peak amplitude with photon irradiation time for the occupied and unoccupied spectra, for the peaks labeled in (a) and (b), is presented in (c) and (d), respectively. A similar plot for the amplitude of the peaks in the second-order C 1*s* spectra, extracted from the same resonant photoemission data, is presented in (e) with the peaks labeled as in Fig. 2(c).

scale). By looking at this feature when it lies above the Fermi level, and fitting the component peaks shown in Fig. 2(b), we can determine the variation in chemical structure with photon irradiation time. The position of the G_{Ca} XPS peak was used to provide the "zero" for the photon energy axis of the NEXAFS spectra in the conversion to initial state energy. Calibration of the Fermi level is done by looking for the crossing of the low-photon Auger emission edge and the second-order core level. This approach allows us then to investigate the chemical variations (second-order core level), occupied states (angle-integrated photoemission), and unoccupied states (NEXAFS) as a function of photon irradiation time in a single measurement.

1. Low-intensity irradiation

The results of the low-intensity photon irradiation measurements performed in a F-G/H-SiC sample are shown in Fig. 6 and are representative of those obtained on the other substrates. Angle-integrated photoemission and NEXAFS measurements are presented in Figs. 6(a) and 6(b) from before (dashed lines) and after (solid lines) irradiation. Component peaks, based on the location of the assigned peaks in Fig. 5, were fitted to both the occupied and unoccupied states at each of the four irradiation time intervals obtained. An example of the fitting is shown for the spectra after irradiation in Figs. 6(a) and 6(b), with the fluorinated graphene σ/bonding π (solid black line), F derived (purple line), and localized dangling π bond (red line) components highlighted. No variation of the fitted amplitude of the dashed component peaks in Figs. 6(a) and 6(b) was observed, while the fluorinated graphene component peak variation is shown in Figs. 6(c) and 6(d) for the occupied and unoccupied states, respectively. The localized contributions from states (F-G1) show an increase with photon exposure, indicating the generation of localized π states. This transition also results in a slight geometrical shift of the F atom bonding orbitals, and leads to the observed reduction in the F-G4 and F-G5 components [Figs. 6(d) and 6(e)]. The XPS as a function of photon irradiation time also shows an increase in the photon-induced (G_S) component and a corresponding decrease in the nonfluorine bonded C atom components (G_{Ca} and G_{Cb}).

This low-intensity photon variation is technologically important, as it allows for the patterning of semiconducting regions (those exposed to low-intensity photons) with a band gap of ~2.5 eV onto a more insulating sample which has a band gap of ~6.2 eV. As the photon irradiated regions emit blue light under mild heating, this may pave the way to integrated optoelectronics devices. After irradiation, the photon-induced π bands are stable for at least several months, but annealing causes a transition back to the ground state. While the fluorinated graphene structures are stable in air, the low-intensity induced-photon variations are not. We conclude then that low-intensity photon irradiation imparts enough energy into the fluorinated graphene film to raise the system from the ground state to a metastable fluorinated graphene layer which relaxes back to the ground state by annealing or exposure to air. Another important aspect of device manufacture is the ability to pattern metallic regions onto a semiconducting substrate, for the F-G-6$\sqrt{3}$ C/SiC and F-G/ H-SiC samples; this can be achieved by removing fluorine atoms and recovering the metallic graphene π bands, a process that occurs at much higher radiation doses.

2. High-intensity irradiation

To investigate the removal of the fluorine atoms, the samples were exposed to a ~100 μm^2 high-intensity photon beam for several hours. XPS spectra of the C 1*s* and F 1*s* peaks were then obtained as a function of sample position across the photon-exposed regions. An example measurement, from a F-6$\sqrt{3}$ C/SiC sample, is presented in Fig. 7 with the C 1*s* line shown in Figs. 7(a) and 7(b) and the fitted F 1*s* amplitude presented in Fig. 7(c). The irradiated regions (red dashed lines) are characterized by the F 1*s* intensity minima and a distinct change in the C 1*s* spectra. An example C 1*s* spectra from a fluorine-depleted region is shown as the inset to Fig. 7(a). This peak has the characteristic shape of a 6$\sqrt{3}$ C-SiC C1s spectra, and the fitted components as described by Emtsev *et al.* [24] accurately describe this peak.

The ground-state electronic structure, with a band gap of ~6.2 eV, can thus be modified to give a semiconducting (band gap of ~2.5 eV) region or a metallic graphene region by photon irradiation. Currently, electronic circuits are patterned using lithographic techniques at the nanometer scale, making this material technologically important. It is also expected that the use of different functional groups, in place of the F, will produce different band gaps between localized energy levels. This is already evidenced by the case of 6$\sqrt{3}$ C-SiC where

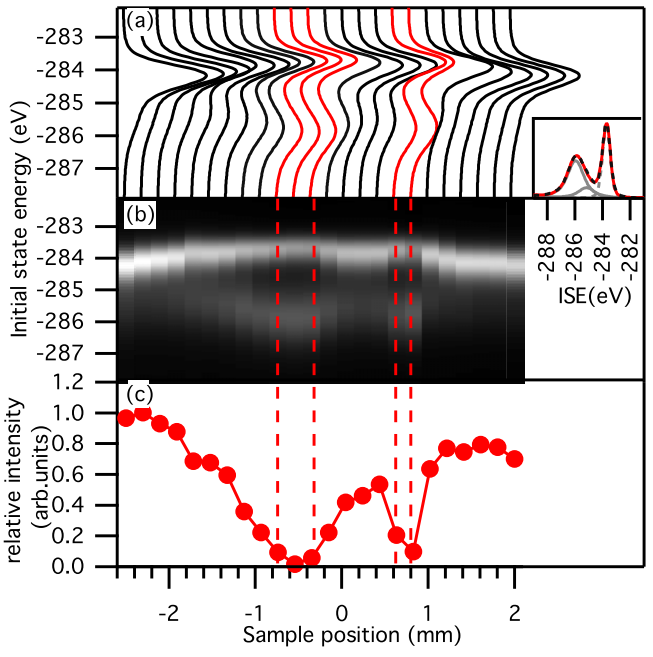

FIG. 7. The C 1*s* spectra stack plot (a) and intensity plot (b), as a function of sample position, across two regions (position ~−0.5 mm and ~7 mm) of a F-6$\sqrt{3}$ C/SiC sample that have been exposed to high-photon radiation doses over several hours. The corresponding amplitude of the F 1*s* peak is shown in (c). The inset to (a) contains an example C 1*s* spectra (solid, red) from the fluorine-depleted regions [red spectra in (a)] with the standard fit [24] (dashed, black) consisting of two 6$\sqrt{3}$ C peaks (solid, gray) and a substrate peak (dotted gray).

these bands not only have a much smaller separation (∼1 eV) but the upper one is shifted below the Fermi level. Calculations also show that replacing F with H should result in a reduced band gap between these localized bands (∼1 eV), but also, and more importantly, the levels should be spin polarized producing a half-metal [20].

IV. CONCLUSION

The electronic, chemical, and physical structure of half-fluorinated graphene on three different substrate interfaces has been determined. Fluorine is bonded to one sublattice of the graphene, which results in σ bands, bonding π bands, and nonbonding localized π states. Fermi level pinning acts to align the band gaps of the fluorinated graphene and SiC and sets the Fermi level within this gap, while relative shifts in the valence and core levels are attributed to partial metallization and hybridization of localized π orbitals in the graphene layer. These mechanisms are usually associated with organic electronic films, and the localized π bonding states in the current samples are very similar to the HOMO and LUMO levels of such films. Both the energies of the occupied and unoccupied states have been measured, and the results show that σ bonds are relatively unchanged by the fluorination, while the bonding π bands show significantly less dispersion than unfluorinated graphene, as is predicted by calculations. The same mechanisms, usually associated with organic electronic films, explain the electronic structure of the similar $6\sqrt{3}$ C-SiC, where two thirds of one graphene sublattice bond to the substrate.

The ground-state electronic structure, with a band gap of ∼6.2 eV, is modified to give an organic semiconducting (band gap of ∼2.5 eV) region or a metallic graphene region by photon irradiation. Using this process patterning by standard lithographic techniques is possible. It is expected that the use of different functional groups, in place of the F, will produce different band gaps between localized energy levels. The half-fluorinated samples therefore represent the first in an important family of graphene-based materials.

ACKNOWLEDGMENTS

The Advanced Light Source is supported by the Director, Office of Science, Office of Basic Energy Sciences, of the US Department of Energy under Contract No. DE–AC02–05CH11231. Work in Erlangen was supported by the DFG through SPP 1459 “Graphene” and SFB 953 “Synthetic Carbon Allotropes” and by the ESF through the EUROGRAPHENE project GraphicRF. A.L.W. acknowledges support from the Max-Planck-Gesellschaft, the Donostia International Physics Centre, and the Centro de Fisica de Materiales in San Sebastian, Spain, and Brookhaven National Laboratory under US Department of Energy, Office of Science, Office of Basic Energy Sciences, Contract No. DE-SC0012704. This work was supported by the Flemish Science Foundation (FWO-Vl) and the Methusalem foundation of the Flemish government. Computational resources were provided by TUBITAK ULAKBIM, High Performance and Grid Computing Center (TR-Grid e-Infrastructure), and HPC infrastructure of the University of Antwerp (CalcUA), a division of the Flemish Supercomputer Center (VSC), which is funded by the Hercules foundation. H.S. is supported by a FWO Pegasus-Long Marie Curie Fellowship, and J.K. by a FWO Pegasus-Short Marie Curie Fellowship. Y.J.C. acknowledges support from the National Research Foundation of Korea under Grant No. NRF-2014R1A1A1002868. The authors gratefully acknowledge the work of T. Seyller’s group at the Institut für Physik, Technische Universität Chemnitz, Germany for providing the samples.

[1] K. S. Novoselov, A. K. Geim, S. V. Morozov, D. Jiang, Y. Zhang, S. V. Dubonos, I. V. Grigorieva, and A. A. Firsov, Science **306**, 666 (2004).
[2] A. K. Geim and K. S. Novoselov, Nat. Mater. **6**, 183 (2007).
[3] A. Bostwick, T. Ohta, J. McChesney, T. Seyller, and E. Rotenberg, Solid State Commun. **143**, 63 (2007).
[4] S. Y. Zhou, D. A. Siegel, A. V. Fedorov, and A. Lanzara, Phys. Rev. Lett. **101**, 086402 (2008).
[5] A. Bostwick, J. L. McChesney, K. V. Emtsev, T. Seyller, K. Horn, S. D. Kevan, and E. Rotenberg, Phys. Rev. Lett. **103**, 056404 (2009).
[6] A. Bostwick, F. Speck, T. Seyller, K. Horn, M. Polini, R. Asgari, A. H. MacDonald, and E. Rotenberg, Science **328**, 999 (2010).
[7] I. Crassee, J. Levallois, A. L. Walter, M. Ostler, A. Bostwick, E. Rotenberg, T. Seyller, D. van der Marel, and A. B. Kuzmenko, Nat. Phys. **7**, 48 (2010).
[8] J. Yan, Y. Zhang, P. Kim, and A. Pinczuk, Phys. Rev. Lett. **98**, 166802 (2007).
[9] P. Denis, Chem. Phys. Lett. **492**, 251 (2010).
[10] F. Rana, IEEE Trans. Nanotechnol. **7**, 91 (2008).
[11] N. Koch, J. Phys.: Condens. Matter **20**, 184008 (2008).
[12] M. Jung, U. Baston, G. Schnitzler, M. Kaiser, J. Papst, T. Porwol, H. J. Freund, and E. Umbach, J. Mol. Struct. **293**, 239 (1993).
[13] S. Duhm, A. Gerlach, I. Salzmann, B. Bröker, R. L. Johnson, F. Schreiber, and N. Koch, Org. Electron. **9**, 111 (2008).
[14] K. P. Loh, Q. Bao, G. Eda, and M. Chhowalla, Nat. Chem. **2**, 1015 (2010).
[15] A. L. Walter, H. Sahin, K.-J. Jeon, A. Bostwick, S. Horzum, R. Koch, F. Speck, M. Ostler, P. Nagel, M. Merz, S. Schuppler, L. Moreschini, Y. J. Chang, T. Seyller, F. M. Peeters, K. Horn, and E. Rotenberg, ACS Nano **8**, 7801 (2014).
[16] C. Berger, Z. Song, T. Li, X. Li, A. Y. Ogbazghi, R. Feng, Z. Dai, A. N. Marchenkov, E. H. Conrad, P. N. First, and W. A. de Heer, J. Phys. Chem. B **108**, 19912 (2004).
[17] K. V. Emtsev, A. Bostwick, K. Horn, J. Jobst, G. L. Kellogg, L. Ley, J. L. McChesney, T. Ohta, S. A. Reshanov, J. Rohrl, E. Rotenberg, A. K. Schmid, D. Waldmann, H. B. Weber, and T. Seyller, Nat. Mater. **8**, 203 (2009).
[18] M. Ostler, F. Speck, M. Gick, and T. Seyller, Phys. Status Solidi B **247**, 2924 (2010).
[19] J. Zhou, Q. Liang, and J. Dong, Carbon **48**, 1405 (2010).

[20] J. Zhou, Q. Wang, Q. Sun, X. S. Chen, Y. Kawazoe, and P. Jena, Nano Lett. **9**, 3867 (2009).
[21] J. O. Sofo, A. S. Chaudhari, and G. D. Barber, Phys. Rev. B **75**, 153401 (2007).
[22] D. Boukhvalov and M. Katsnelson, J. Phys.: Condens. Matter **21**, 344205 (2009).
[23] R. R. Nair, W. Ren, R. Jalil, I. Riaz, V. G. Kravets, L. Britnell, P. Blake, F. Schedin, A. S. Mayorov, S. Yuan, M. I. Katsnelson, H.-M. Cheng, W. Strupinski, L. G. Bulusheva, A. V. Okotrub, I. V. Grigorieva, A. N. Grigorenko, K. S. Novoselov, and A. K. Geim, Small **6**, 2877 (2010).
[24] K. V. Emtsev, F. Speck, Th. Seyller, L. Ley, and J. D. Riley, Phys. Rev. B **77**, 155303 (2008).
[25] C. Riedl, C. Coletti, T. Iwasaki, A. A. Zakharov, and U. Starke, Phys. Rev. Lett. **103**, 246804 (2009).
[26] F. R. McFeely, J. F. Morar, N. D. Shinn, G. Landgren, and F. J. Himpsel, Phys. Rev. B **30**, 764 (1984).
[27] F. Withers, M. Dubois, and A. K. Savchenko, Phys. Rev. B **82**, 073403 (2010).
[28] J. T. Robinson, J. S. Burgess, C. E. Junkermeier, S. C. Badescu, T. L. Reinecke, F. K. Perkins, M. K. Zalalutdniov, J. W. Baldwin, J. C. Culbertson, P. E. Sheehan, and E. S. Snow, Nano Lett. **10**, 3001 (2010).
[29] K.-J. Jeon, Z. Lee, E. Pollak, L. Moreschini, A. Bostwick, C.-M. Park, R. Mendelsberg, V. Radmilovic, R. Kostecki, T. J. Richardson, and E. Rotenberg, ACS Nano **5**, 1042 (2011).
[30] G. Kresse and J. Hafner, Phys. Rev. B **47**, 558 (1993).
[31] G. Kresse and J. Furthmüller, Phys. Rev. B **54**, 11169 (1996).
[32] P. E. Blöchl, Phys. Rev. B **50**, 17953 (1994).
[33] G. Kresse and D. Joubert, Phys. Rev. B **59**, 1758 (1999).
[34] J. P. Perdew, K. Burke, and M. Ernzerhof, Phys. Rev. Lett. **77**, 3865 (1996).
[35] S. Grimme, J. Comput. Chem. **27**, 1787 (2006).
[36] W. Tang, E. Sanville, and G. Henkelman, J. Phys.: Condens. Matter **21**, 084204 (2009).
[37] T. Seyller, K. Emtsev, K. Gao, F. Speck, L. Ley, A. Tadich, L. Broekman, J. Riley, R. Leckey, O. Rader, A. Varykhalov, and A. Shikin, Surf. Sci. **600**, 3906 (2006).
[38] J. Sivek, O. Leenaerts, B. Partoens, and F. M. Peeters, J. Phys. Chem. C **116**, 19240 (2012).
[39] J. A. Carlisle, T. Miller, and T.-C. Chiang, Phys. Rev. B **49**, 13600 (1994).
[40] D. G. de Oteyza, J. M. García-Lastra, M. Corso, B. P. Doyle, L. Floreano, A. Morgante, Y. Wakayama, A. Rubio, and J. E. Ortega, Adv. Funct. Mater. **19**, 3567 (2009).
[41] J. Binner and Y. Zhang, J. Mater. Sci. Lett. **20**, 123 (2001).
[42] J. Tersoff, Phys. Rev. B **30**, 4874 (1984).
[43] J. J. Yeh and I. Lindau, *Atomic Data and Nuclear Data Tables*, Atomic Subshell Photoionization Cross Sections and Asymmetry Parameters: $1 \leqslant Z \leqslant 103$, Vol. 32 (Academic, New York, 1985).
[44] J. Zhou, M. M. Wu, X. Zhou, and Q. Sun, Appl. Phys. Lett. **95**, 103108 (2009).
[45] O. Leenaerts, H. Peelaers, A. D. Hernández-Nieves, B. Partoens, and F. M. Peeters, Phys. Rev. B **82**, 195436 (2010).
[46] A. Ramasubramaniam, Phys. Rev. B **81**, 245413 (2010).
[47] C. E. Junkermeier, S. C. Badescu, and T. L. Reinecke, arXiv:1302.6878v1.
[48] R. Saito, G. Dresselhaus, and M. S. Dresselhaus, *Physical Properties of Carbon Nanotubes* (Imperial College Press, Tokyo, 1998).
[49] D. K. Samarakoon and X.-Q. Wang, ACS Nano **3**, 4017 (2009).